# Position Control of a Novel Planar Switched Reluctance Motor

Jianfei Pan[1] Student Member, IEEE Norbert C. Cheung[2] Member, IEEE and Jinming Yang[3]

[1, 2]Jianfei Pan and Norbert C. Cheung, Department of Electrical Engineering, Hong Kong Polytechnic University, Hunghom, Kowloon, Hong Kong, e-mail : eencheun@polyu.edu.hk
[3] Jinming Yang, Electric Power College, South China University of Technology, Guangzhou, China.
e-mail: jmyang@scut.edu.cn

*Abstract*—**This paper presents the position control of a novel 2D switched reluctance (SR) planar motor. The planar motor consists of a 6-coil moving platform, and a flat stator base made from laminated mild steel blocks. Unlike conventional X-Y tables, which stack two moving slides on top of each other, the proposed 2D planar motor has the advantages of simple mechanical construction, high reliability, and is able to withstand harsh operating conditions. Together with the two linear encoders attached to the X and Y axes, the motor can be controlled under closed loop mode. To combat the problem of force nonlinearity, this paper proposes a cascade controller with force linearization technique to implement the drive controller. Due to the unique structure of the magnetic circuit, there is very little coupling between the X- and Y-axis, and no decoupling compensation is needed. Preliminary control results show that the proposed VR planar driver has a positional accuracy of 5 microns and an acceleration/deceleration rate of 2G.**

## I. Introduction

In industry, precise motion control for two dimensions is in high demand. This is often achieved by d.c. or a.c. motors as the prime motion actuator, and couple their outputs shafts to mechanical motion translators (e.g. reduction gear, belt, ball screw, etc.) with mechanical slides, stacked on top of each other to form an X-Y table. Though this is the most widely used method, it has disadvantages of reduced accuracy, complex mechanical structure, difficult adjustments and alignments, high production cost, and low reliability.

To overcome the above problems, a few direct-drive planar solutions have been proposed.

Sawyer motor [1, 2] is the first and the only practical type of planar motor available to industry. Though it can provide uniform performance over the entire workspace and offer fairly high speeds, due to its open loop nature, it is susceptible to loss of steps, when it is subject to external disturbances.

Planar motors based on permanent magnets are proposed by [3-5]. In [3], permanent magnets are located in the base and organized as a checkerboard arrangement. The mover has eight coils installed on two linear guides. Another scheme [4, 5] shows an intercalated arrangement of coils for the moving platform, and the mover is composed of two high-energy permanent magnets fixed on trucks. It has three degree-of-freedom. Planar motors based on permanent magnets have complicated structures, and the utilization factor of the magnets is quite low. Besides, the manufacturing and maintenance cost is high and complex.

In this paper, a novel planar motor based on switched reluctance principle is introduced [6]. The manufacturing cost of switched reluctance actuator is much lower than similar permanent magnetic devices. The proposed actuator has a very simple structure with few mechanical parts, and it can be manufactured easily. Since the motion system is a self-aligned direct drive system, there is no need for X-Y alignments or rotary-to-linear couplings.

At present, linear motion system based on switch reluctance (SR) principle is mainly for transportation systems and the control output is velocity. A linear SR actuator whose control output is targeted on position control has already been constructed in our laboratory [7, 8]. The linear SR motor can achieve micron precision and high acceleration rates. The construction of a directly driven two-dimensional SR motor is a logical continuation from the previous idea.

The purpose of this paper is to focus on the characteristics and modeling of the planar SR motor, and the construction of a nonlinear cascade controller for the motor. The development of the planar motor, and its special magnetic circuit characteristics, will be reported in another paper.

The organization of this paper is as follows: the design and construction is introduced in section II. Section III focuses on the motor's parameters and characteristics. Section IV proposes a cascade control scheme with nonlinear lookup tables. Section V describes the implementation of the planar SR motor drive system and the results obtained.

## II. Construction of the Plan

Fig. 1 shows the photo of the planar SR motor. It is based on the "straightened-out" version of a 6/4 pole rotary switched reluctance motor, along the X and Y directions.

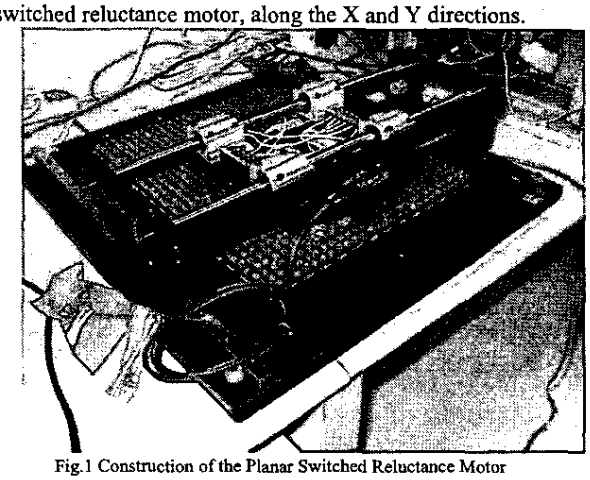

Fig.1 Construction of the Planar Switched Reluctance Motor

0-7803-8730-9/04/$20.00 ©2004 IEEE

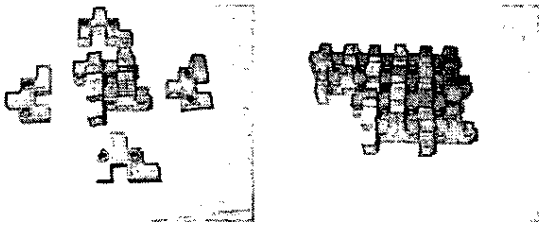

(a) (b)

Fig.2 Stator elements and structure

Since the motor is two dimensional, the stator plate consists of square extrusion blocks, instead of rectangular extrusion toothed rail, as in the case of linear SR motor. Two roller slides are employed to support the movement in X direction, and another pair of linear guides is attached to the base to enable the motor for the movement of Y direction.

Instead of carving the square extrusions from a single slab of steel, the base plate is constructed from small pieces of "laminated steel blocks", as shown in Fig. 2 (a) and (b). The blocks are held together by epoxy glue.

This method of construction can reduce the manufacturing cost and simplify the overall construction complexity. Moreover, the same laminated blocks can be used to construct different sizes of base plates, according to different requirements and applications.

Two sets of 3-phase coil windings with wide magnetic teeth are employed on the moving platform. Altogether there are 6 coils, with 3 coils responsible for each direction. All six coils have the same dimensions and ratings. By increasing the coil-teeth width, and making its dimensions to be exactly the same multiple of the teeth pitch, cross couplings of X-Y force can be minimized. Fig. 3 shows the coil structure.

Two sets of 3-phase flux decoupled winding arrangement with longitudinal configuration are chosen because of the following advantages:

a. The decoupled flux windings lead to a simpler motor model due to zero mutual inductance.

b. The individual phase windings reduce the manufacturing cost and complexity.

c. Long travel distance can be accomplished easily by combining longitudinal track guides.

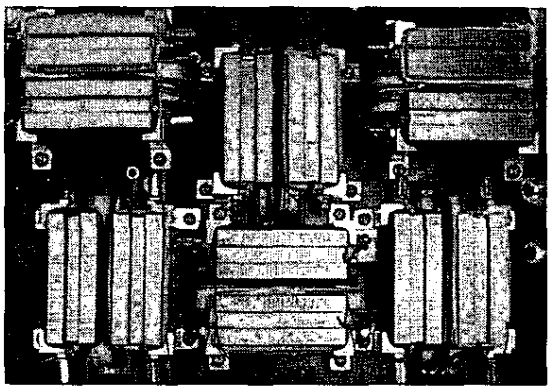

Fig.3 Two sets of three phase coils, in the X and Y directions

Table 1 Parameters of the planar motor

| | |
|---|---|
| Pole pitch | 6 mm |
| Air gap | 0.55mm |
| Number of turns per phase | 160 |
| Rate power | 120W |
| Phase resistance | 1.5Ω |
| Size of base plate | 450×450mm |
| Travel distance | 300×300mm |
| Mover size | 250×220mm |
| Encoder precision | 0.5 μm |

Table 1 shows the major dimensions and important parameters of the planar SR motor. The original intention was to use the planar motor to replace an X-Y table with a traveling range of 300mm by 300mm. However, the planar SR motor can be reconfigured to larger or smaller sizes, using the same principles and calculations.

## III. Characteristics of the Planar Motor

The nonlinear equations governing switched reluctance principle (for the $K_{th}$ phase of one direction) is:

$$V_k(t) = R_k i_k(t) + \frac{\partial \lambda_k(i_k(t), x(t))}{\partial x(t)} \frac{dx(t)}{dt} + \frac{\partial \lambda_k(i_k(t), x(t))}{\partial i_k(t)} \frac{di_k(t)}{dt}$$

and $\lambda_k = \lambda_{kj} + \lambda_{km} + \lambda_{ke}$ (1)

where $V_k(t)$, $i_k$ and $R_k$ are the phase voltage, phase current, and phase resistance respectively. $x(t)$, $\lambda_k$ is the position and the total flux linkage, respectively [9]. The flux linkage $\lambda_k$ composes of self flux linkage $\lambda_{kj}$, mutual flux linkage $\lambda_{km}$, and leakage flux $\lambda_{ke}$. On the mechanical side, the force of the motor can be represented as:

$$f_{x(y)}(i_a(t), i_b(t), i_c(t), x(t)) = \sum_{k=a}^{c} f_k(i_k(t), x(t)) = M_m \frac{d^2x(t)}{dt^2} + B_m \frac{dx(t)}{dt} + f_l(t) \quad (2)$$

where $f_{x(y)}(i_a(t), i_b(t), i_c(t), x(t))$ is the total generated electromechanical force of one axis, $f_l(t)$ is the external load force, and $M_m$ and $B_m$ are the mass and the friction constant, respectively.

The flux linkage profile is measured using the "search coil" method [10]. An AC current from an isolated autotransformer ranged from 1A~50A is fed into the main coil. By measuring the induced voltage across the search coil, flux linkage can be calculated according to the equation below:

$$\varphi(t) = -\frac{1}{N_s} \int e(t) \cdot dt \quad (3)$$

where $e(t)$ is the voltage induced by the flux.

Then flux linkage can be calculated as:

$$\lambda(t) = n \cdot \varphi(t) \quad (4)$$

where $n$ is the number of turns of the stator winding.

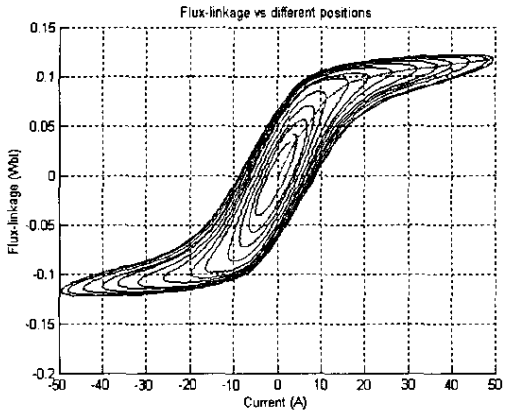


Fig.4 Hysteresis loops at different current levels

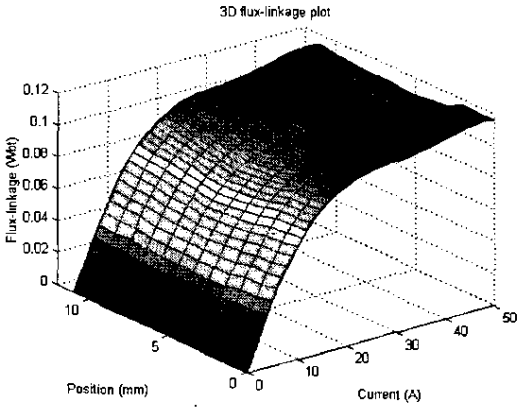


Fig.5 Flux linkage versus current and position for the motor

Fig. 4 shows the flux linkage hysteresis loops of this planar motor at different current levels at minimum air gap distance. The loop areas are quite substantial at this position. However, it was found that, when the teeth of the mover and the stator are not fully aligned, the hysteresis loop area will decrease drastically, and it will not place a big stress on the controller. Therefore a hysteresis controller is not required in the final control algorithm.

Fig. 5 shows the 3D plot flux linkage profile at different current and position levels. The plot is constructed by joining the vertex of the hysteresis loops measurements at different current levels and positions. The last important set of parameter of the motor is the force output at different positions and current levels.

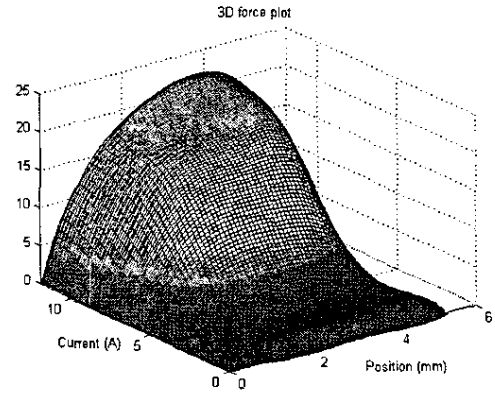


Fig.6 Force versus current and position

This set of data can be obtained by calculating the co-energy from the flux linkage data, or by direct measurement. To achieve accurate measurement at precisely each predetermined locations, a test rig fixture is constructed. The test fixture can accurately divide one pole width (6mm) into 50 different equally spaced divisions. Once the moving platform is fixed into place, different current values (0~15A) are injected to the phase winding. After this, the motor's force is measured by a load cell sensor, which then feeds the force values directly to the computer. Since the phase windings are magnetically decoupled and the mechanical parameters are identical, only one phase of measurement is needed. Fig. 6 shows the 3D plot of force versus current and position.

## IV. THE CONTROL STRATEGY

Exploiting the fact that the current dynamics is at least an order faster than the mechanical dynamics, this paper proposes a dual rate cascade control approach. A fast inner loop current controller is employed to regulate the current-voltage nonlinearity of the actuator, while a slower outer loop trajectory controller is used to control the mechanical dynamics. On top of this, a nonlinear function is included to compensate the nonlinearity of force against current and position. Figure 7 is the overall block diagram of the control system.

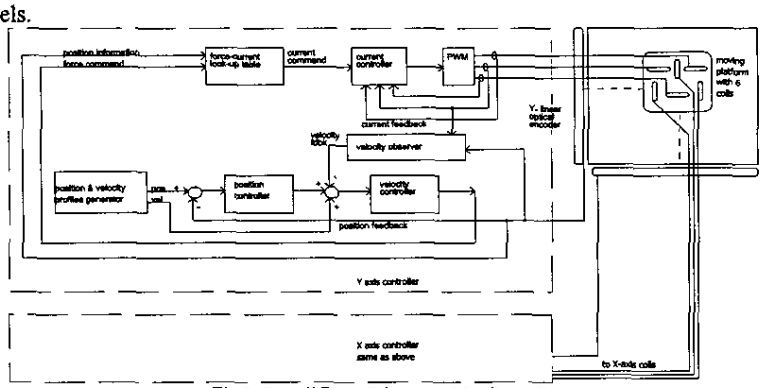


Fig.7 Overall Block Diagram of the Controller

In Fig. 7 the current controller is employed to linearize the current-voltage relation of the actuator. A simple PI controller is proposed. Position can be assumed to be stationary during the control time frame of the current controller, since current dynamics are much faster than mechanical dynamics. The nonlinear function bridges the link between the trajectory controller and the current controller. It receives force commands and position information, and outputs desired current set points to the current controller.

Since the relations of force, current, and position are nonlinear in nature, a 2D force current position lookup table is used to describe the nonlinear force profile.

The trajectory controller forms the essential part of the slow subsystem. It is a typical PID controller. The controller's operation is based on the assumption that the current controller has perfect tracking capability, and the nonlinear function mapper generates the linearized current command to the current controller.

To find out the inverse relationship between current, force and position, another experiment has been conducted by fixing the moving platform at the corresponding 50 positions within one pole width, and then measure the currents required to generate the desired force.

In the measurement of force, it is found that X-Y force coupling contribute less than 1% of the total force generated. Therefore the inter-axis coupling force is considered insignificant, and it can be easily corrected by the individual controller of the X-axis and the Y-axis. As shown in Fig. 7, the control scheme is the same for X- and Y- axis of direction and each is controlled independently.

For the implementation of the inverse force current position lookup tables, continuity and smoothness of the profile are more important than accuracy. Therefore we use a relatively low 27×27 element to build up the lookup tables for the force compensation values. To ensure the smoothness, a two-dimensional linear interpolation scheme is implemented for the intermediate values. This produces a considerably low worst-case deviation from the original nonlinear function and the output values can also follow a smooth profile. A 27×27-element lookup table with two-dimensional linear interpolation is sufficient to describe the force profile with an accuracy of ±5%.

Table 2 shows the method of obtaining the required current $i^*$ by bilinear interpolation method. Firstly, from the position input $x_{in}$ and force command $F_{in}$, two pairs of data $i(F_1, x_1)$ and $i(F_2, x_1)$ in the lookup table are located. For each pair, a linear interpolation is done according to the ratio of $F_1$, $F_2$ and $F_{in}$. As a result, two intermediate elements, $i(F_{1\text{-}2}, x_1)$ and $i(F_{1\text{-}2}, x_2)$ are obtained. Finally, the output current command $i^*$ is obtained by interpolating the two intermediate elements with $x_1$, $x_2$ and $x_{in}$.

For each direction, before the lookup table control module, a commutation judgment mechanism is inserted to generate the 3-coupled force command. For example, if the current position falls into 5 and the required force command is a negative value, then phase B and C will be energized to produce the required force command; on the contrary, if the force command is a positive value, then only phase A will be energized to generate the command force. Here we use a simple linear force distribution method if two phases are simultaneously excited. Table 3 shows the distribution table if the force command is positive.

Table 2 Phase excitation table (0mm= Phase A at fully aligned position)

| Region | Position range(mm) | +ve force command | -ve force command |
|---|---|---|---|
| 1 | 0—2 | B | C,A |
| 2 | 2—4 | B,C | A |
| 3 | 4—6 | C | A,B |
| 4 | 6—8 | C,A | B |
| 5 | 8—10 | A | B,C |
| 6 | 10—12 | B,A | C |

Table 3 Force Distribution table for positive force command

| Region | Force for Phase A | Force for Phase B | Force for Phase C |
|---|---|---|---|
| 1 (0-2 mm) | 0 | $f_{in}$ | 0 |
| 2 (2-4 mm) | 0 | $f_{in}\times[1-\frac{1}{2}(x_{in}-2)]$ | $f_{in}\times[\frac{1}{2}(x_{in}-2)]$ |
| 3 (4-6 mm) | 0 | 0 | $f_{in}$ |
| 4 (6-8 mm) | $f_{in}\times[\frac{1}{2}(x_{in}-6)]$ | 0 | $f_{in}\times[1-\frac{1}{2}(x_{in}-6)]$ |
| 5 (8-10mm ) | $f_{in}$ | 0 | 0 |
| 6 (10-12m) | $f_{in}\times[1-\frac{1}{2}(x_{in}-10)]$ | $f_{in}\times[\frac{1}{2}(x_{in}-10)]$ | 0 |

## V. Implementation and Result

The experiment is implemented on a dSPACE DS1104 DSP motion controller card. This card has an on-board 250MHz DSP for real-time computation and interfaces with PC by PCI bus. It consists of two sets of 24-bits incremental encoder input channels, six 12-bit ADC channels for analog inputs and six 12-bit DAC channels for analog outputs. This DSP control card directly interfaces "real-time workshop" of MATLAB and control parameters can be modified online. C codes can be complied and downloaded directly to the DSP.

Fig. 8 shows the step response of the current. The current response is slower at the fully aligned position, when the inductance of the motor is the greatest. The current response is faster at the unaligned position, when the coil inductance is reduced. Overall the settling time is less than 1ms, which is much faster than the mechanical time constant. There is no instability in any current level or position.

Fig. 9 shows the dynamic performance of the motor when it is tracking a saw-tooth wave and a square wave. For long distance travel, some overshoot appears. However, the motor settles within 500ms under all conditions.

Fig. 10 shows the performance of the motor when it is drawing a circle. Overall the motor can track a circular trajectory path quite satisfactory. However, the dynamic errors of some places can be as high as 0.6mm. This may be due to the fact of uneven mechanical frictions at some portions of the track.

When maximum current of 20A is injected into the coils

the maximum acceleration if 2G can be achieved. For point to point repeatability testing, an accuracy of 5 microns is achieved.

## VI. Conclusion

This paper has described a novel planar motion system which uses a simple and robust SR planar motor. The manufacturing procedure for the 2D SR planar motor is simple and straight forward: the moving platform houses 6 coils which can be made by coil winding machine individually. The base plate is constructed from small laminated blocks which can be manufactured individually. On top of this, there is no need for the costly and complicated motor components of magnets, commutators, and complex windings.

In this project, a cascade controller with a 2D linearization table is employed to produce precise and uniform force output from the 2D SR planar motor. Due to the clever design, there is very little cross-coupling between the X and Y axis; therefore a force decoupler is not necessary for the control of the planar motor. Preliminary results show that the motor can be controlled to a positional accuracy of 5 microns and an acceleration rate of 2G under normal load.

The proposed VR planar motion system is therefore an ideal replacement for traditional X-Y tables in industrial automation applications.

## VII. Acknowledgement

The authors would like to thank the Hong Kong Research Grants Council for the sponsoring of this research project under the project code B-Q473 and National Natural Science Foundation of China (60174025).

## VIII. Reference

[1] B.A. Sawyer, "Magnetic positioning device", U.S. Patent 3,457,482, July 1969.

[2] E.R. Pelta, "Two-axis sawyer motor for motion systems", IEEE Control Systems Mag., Oct 1987.

[3] D. Ebihara and M. Watada. "Study of a Basic Structure of Surface Actuator." IEEE Trans. on Magnetics, Vol.25, No.5, pp.3916-3918, September 1989.

[4] A. F. Flores Filho, A. A. Susin, M. A. da Sliveira. "Development of a Novel Planar Actuator."

[5] Junichi Tsuchiya and Gunji Kimura. "Mover Structure and Thrust Characteristic of Moving-Magnet-type Surface Motor."

[6] N.C. Cheung, J.F. Pan, J.M. Yang, "Two Dimensional Variable Reluctance Planar Motor," U.S. Patent (filed: May 2004).

[7] W.C. Gan, N.C. Cheung, "Development and Control of a Low-cost Linear Variable reluctance Motor for Precision Manufacturing Automation," IEEE/ASME Transactions on Mechatronics, p 326 -333, Vol. 8, Issue 3, Sep 2003.

[8] W.C. Gan, N.C. Cheung, Q Li, "Position Control of Linear Switched Reluctance Motors for High Precision Applications," IEEE Transactions on Industry Applications, p 1350-1362, Vol. 39, Iss. 5, Sep/Oct 2003.

[9] T.J.E. Miller, "Switched reluctance motor and their control", Magnet Physics Publishing and Clarendon Press, Oxford, 1993.

[10] K.K.C. Chan, N.C. Cheung, "Modelling and Characterisation of a Novel Two-Finger Variable Reluctance Gripper," ISA Transactions (accepted for publication 12 Feb 2004).

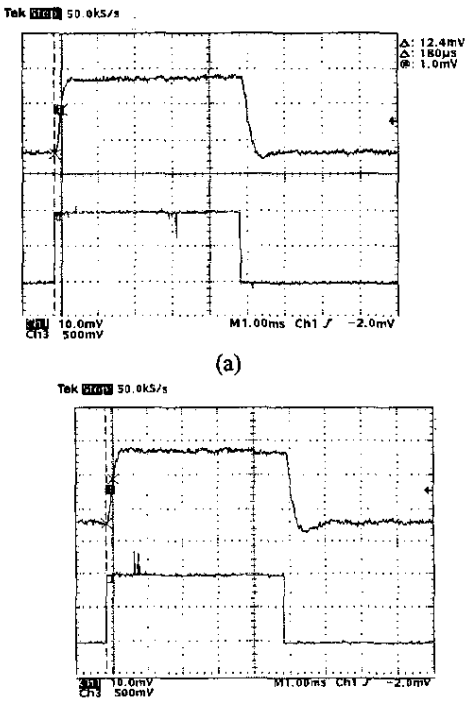


Fig.8 Current response of the motor's coil at (a) fully aligned position, and at (b) fully unaligned position.

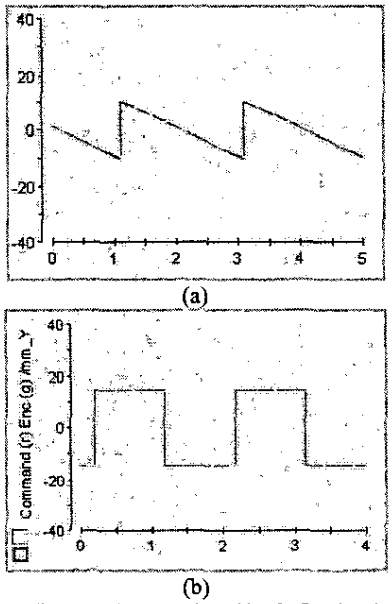


Fig.9 Large distance trajectory path tracking for X axis only. (a) Saw tooth path, and (b) Pulsed rectangular path. (Y axis: mm; X axis: *seconds*)

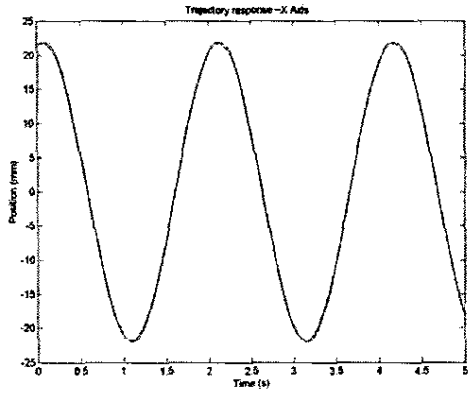


(a)

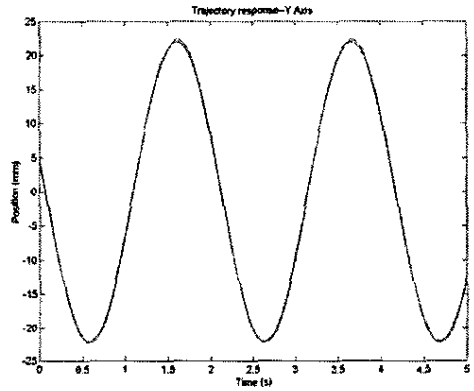


(b)

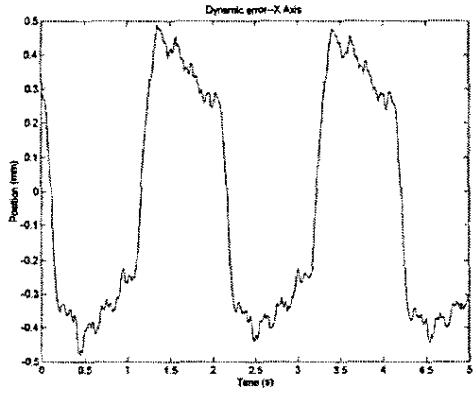


(c)

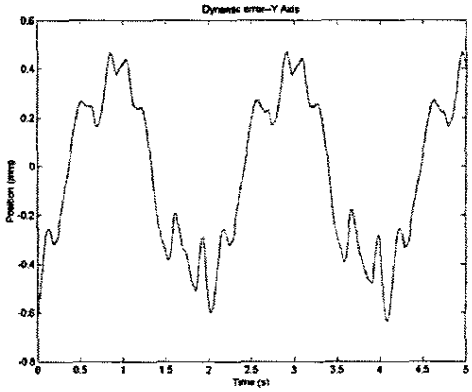


(d)

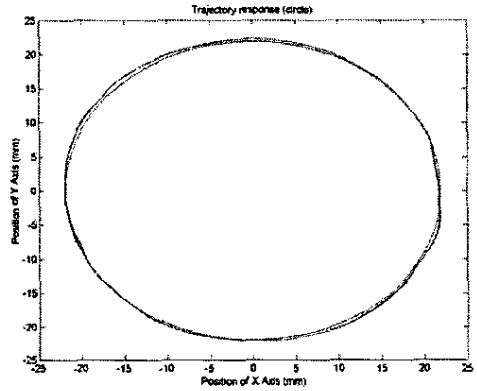


(e)

Fig.10 Trajectory response of the planar SR motor for circular motions. (a) Y axis of the motor under sinusoidal path command (Y axis: mm; X axis: s); (b) X axis of the motor under sinusoidal path command (Y axis: mm; X axis: s); (c) Tracking error of motor's Y axis (Y axis: mm; X axis: s); (d) Tracking error of motor's X axis (Y axis: mm; X axis: s); (e) The overall 2D trajectory path (Y and X axis: mm)